Transworld Research Network
37/661 (2), Fort P.O., Trivandrum-695 023, Kerala, India

Recent Res. Devel. Applied Phys., 5(2002): 313-338 ISBN: 81-7895-047-2

Advancement of bismuth layer structured ferroelectrics through substitution / doping and other processing

Yun Wu[1], Steven J. Limmer and Guozhong Cao*
Department of Materials Science and Engineering, University of Washington, Seattle, WA 98195, USA
*E-mail : gzcao@u.washington.edu

Abstract

This article reviews the studies on bismuth layer structured ferroelectrics (BLSFs), focusing on the most widely reported strontium bismuth tantalate niobate $SrBi_2(Ta, Nb)_2O_9$ (SBTN) and bismuth titanate $Bi_4Ti_3O_{12}$ (BIT) systems. Through partial substitution or doping, the crystal structure, microstructure and electrical, dielectric and ferroelectric properties of BLSFs could be appreciably modified. In addition, the crystalline orientation, grain size effect, and post-annealing effects on the ferroelectric properties are discussed.

[1] Present address: Advanced Micro Devices Inc. Sunnyvale, CA 94086, USA. E-mail: wuyun33@hotmail.com

Correspondence/Reprint request: Dr. Steven J. Limmer, Department of Materials Science and Engineering, University of Washington, Seattle, WA 98195, USA

1. Introduction

Ferroelectrics have attracted research interests for several decades for their potential use as nonvolatile random access memories with fast access time and low power consumption [1-2]. The earlier research focus was on the isotropic perovskite ferroelectrics such as barium titanate [3]. Pb(Zr, Ti)O_3 (PZT) gradually emerged as a promising candidate for this application as it has very high remnant polarization (P_r) [4-6]. Doping effects on both A site and B site of PZT systems were extensively studied [7-11]. However, the problem of fatigue, e.g., the P_r values drop sharply after $10^6 \sim 10^8$ read-write cycles, has been reported as main obstacle for PZT to be used commercially as a high-density nonvolatile memory material [12-13]. In the 1950s, Aurivillius first reported a new family of bismuth layer structured ferroelectrics. BLSFs compounds are generally represented by the following formula

$$(Bi_2O_2)^{2+}(A_{m-1}B_mO_{3m+1})^{2-} \quad (1)$$

where A = Bi, Pb, Na, K, Sr, Ca, Ba, rare earths; B = Ti, Nb, Ta, Fe, Mo, W, Cr; and m is a natural number from 1 to 8 or a fraction such as 2.5 or 3.5 [14-17]. BLSFs have started to attract more research interest because of their promise for better reliability behavior [18-20]. Among these layered ferroelectrics, the $SrBi_2(Ta, Nb)_2O_9$ (SBTN) system has been considered one of the most promising candidates for nonvolatile ferroelectric random access memories (FeRAMs), because of its lack of fatigue after > 10^{10} read-write cycles, and because it is more environmentally friendly (no lead). Mihara et al. published a comprehensive paper comparing the ferroelectric properties of $SrBi_2Ta_2O_9$ (SBT) and the PZT system [21]. Figure 1 shows the comparison of normalized P_r values versus cycle numbers in the two systems [21]. They explained that the advantages of the SBT system over PZT were due to less space charge and inherent domain motion (2 dimensional) in SBT. Another mechanism for this fatigue free property of SBT is from the microstructure point view. A polarization switching mechanism was proposed for explaining fatigue free properties based on the existence of antiphase boundaries (APBs) in SBT. During polarization reversals, new polarization domains nucleate not only at the interface between electrode and ferroelectric capacitors but also at APBs. Providing these extra nucleation positions in the domain switching process helps to realize the polarization reversals in SBT [22-23]. However, the SBTN system also suffers from rather low P_r and high processing temperature [24]. Another widely studied system is BIT because of its high P_r value [25-26]. But BIT does not have the fatigue-free behavior of the SBTN system. The structures of SBTN and BIT are shown in figure 2.

Similar to isotropic perovskites, layer structured perovskites do not have a close packed crystal structure, thus permitting a wide variety (in terms of types of ions and amount) of cations to substitute for either A or B or both ions. Although doping or substitution in perovskite ferroelectrics has less dramatic effects on physical properties than that found in conjugated polymers and semiconductors, doping has been proven to be an effective way adjusting / improving the ferroelectric properties of SBTN and BIT systems. The doping or substitution could be in the bismuth oxide layer and/or in the perovskite-like units (A or B sites). One example of a more complex substitution is the

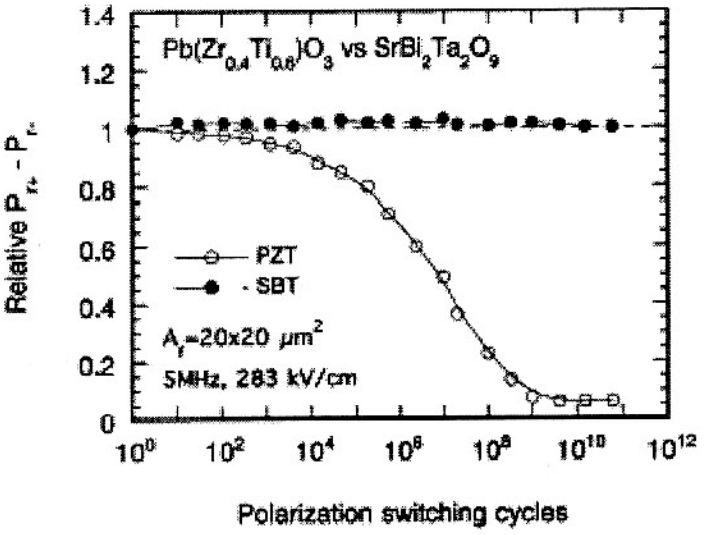

Figure 1. The relative remnant polarization (P_{r+} - P_{r-}) of PZT and SBT as a function of number of switching cycles. The capacitance area was 20x20 μm^2, and the electric field of pulses during fatigue was 283 kV/cm. From C. A. P. Araujo et al. [21]. Reprinted by permission from Japanese Journal of Applied Physics.

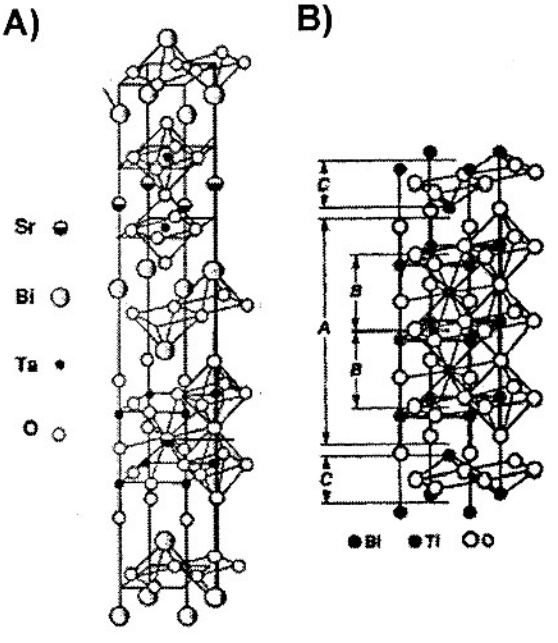

Figure 2. Lattice structures of SBTN (A) and BIT (B).

formation of mixtures of BLSFs compounds with different m values, such as SBTN (m=2) and $SrBi_4Ti_4O_{15}$ (m=4) [27]. In this review, we are focusing mainly on the SBTN and BIT systems. The discussions will include the substitution of A and B sites, and bismuth ions in the buffer oxide layer. Besides substitution/doping effects, we will also discuss the influence of microstructure, such as orientation and grain size effect, and annealing process on the properties of SBTN and BIT systems.

2. Substitution and doping effect

One good example of the doping effect is the electrical conductivity of insulating polyacetylene polymer, which could increase more than 10 million times after adding bromine or iodine [28], and this discovery opens the door of studies and applications of electrically conductive polymers. Doping in pure silicon results in an increase of room temperature electrical conductivity of 5-6 orders of magnitude with ~1ppm level boron [29]. Similar approaches were widely adopted in the research of oxides such as in superconductors [30] and ferroelectrics [31]. Strictly speaking, doping means the ions used for replacement and to be replaced have different chemical valences, while substitution is for same valence ion substitution [31]. Same valence substitution and different valence doping effects in BLSFs will be discussed separately below.

2.1. Same valence substitution

2.1.a. A site ions substitution

In the SBTN system, the A site ions are strontium (Sr^{2+}) ions. Similar ferroelectric systems with other possible A site ions, such as $PbBi_2Nb_2O_9$ was reported by Smolenskii et al. [32]. However, the existence of lead vacancies due to its high volatility made lead substitution unattractive. Naturally, strontium ions might be substituted by their same group elements such as calcium (Ca^{2+}) or barium (Ba^{2+}) ions. Newnham et al. reported the structure of 10 at% of Sr^{2+} substituted by Ba^{2+} in SBT with lower Curie temperature and reduced distortions in the perovskite units [33]. Properties of barium incorporated SBT thin films were also reported [34-35]. $(Na_{0.5}Bi_{0.5})Bi_2Nb_2O_9$ is also reported as a BLSF with sodium and bismuth ions co-substituting Sr^{2+} because both Bi^{3+} and Na^{+} ions have similar ionic radius with Sr^{2+} [36]. We studied the $(Ca_xSr_{1-x})Bi_2Nb_2O_9$ (CSBN) and $(Ba_xSr_{1-x})Bi_2Nb_2O_9$ (BSBN) ceramics with x up to 0.3 [37-38]. XRD analyses indicated single-phase layer structured CSBN and BSBN were formed within the composition ranges studied. The Curie temperatures change linearly with various substitution content (see figure 3). However, the Curie temperatures extrapolated from figure 3 for $BaBi_2Nb_2O_9$ and $CaBi_2Nb_2O_9$, ~90 °C and ~ 910 °C, are quite different from their reported vales, ~200 °C [39] and ~ 620 °C [40], respectively. With the constraints imposed by the bismuth oxide layers, the observed linear relationship at low substitution levels of BSBN and CSBN may not be able to continue throughout the entire composition.

Figure 4 shows that the dc conductivity of $SrBi_2Nb_2O_9$ (SBN) is decreased with increasing concentrations of calcium and barium. For a single phase material with a homogenous microstructure, the electrical conductivity, σ, depends on both the concentration and mobility of charge carriers and can be described by the following equation [41]:

$$\sigma = nq\mu = (A/T)\exp(-E_a/kT) \quad (2)$$

where n is the concentration of charge carriers, q, the number of charges per charge carrier, μ, the mobility of charge carriers, A, a temperature-independent constant, E_a, the

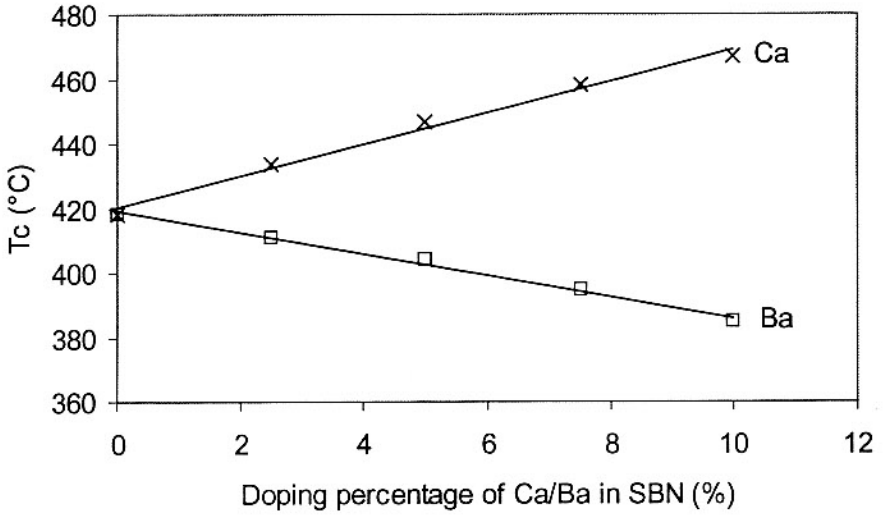

Figure 3. Curie temperature vs. Ca/Ba substitution content in SBN.

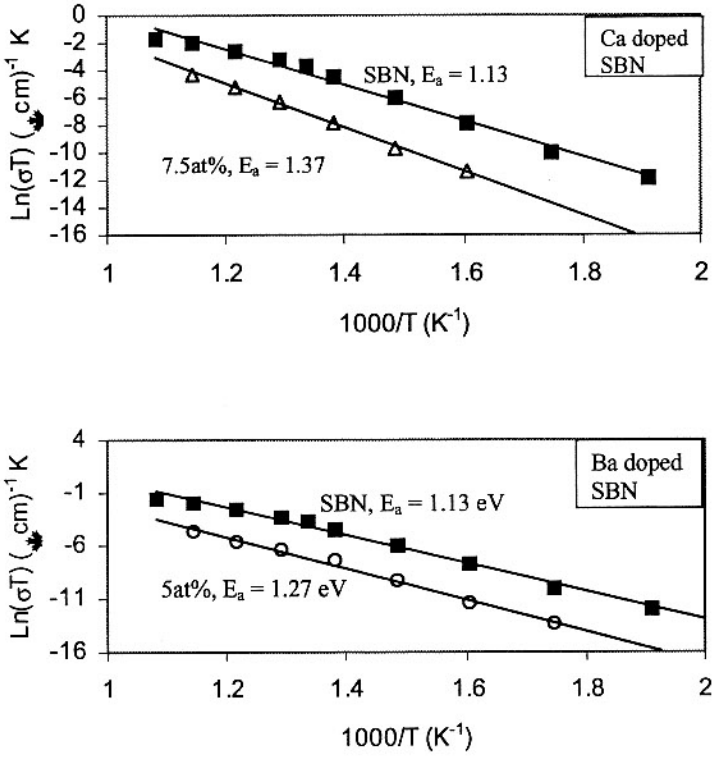

Figure 4. DC conductivity of Ca substituted (a) and Ba substituted (b) SBN ceramics.

nominal activation energy per charge carrier, k, the Boltzmann's constant and T stands for temperature. Judging from the activation energy values (table 1), the migration of oxygen vacancies could be responsible for the conduction [42-44]. However, it is not clear why the activation energy increases with both barium and calcium substitution. It is known that the Ba-O bond (~ 562 kJ/mol) [45] is stronger than, but the Ca-O bond (~402 kJ/mol) [45] is weaker than, the Sr-O bond (~ 426 kJ/mol) [45], so the bond strength

Table 1. DC conductivity and activation energies of SBN and doped samples. X stands for the atomic percentage of substituting ions Ca^{2+} and Ba^{2+} in SBN.

Sample	E_a (eV)	σ_{dc} at 500 °C (S/cm)
SBN (X=0)	1.13	~4.84×10^{-5}
CSBN (X=7.5%)	1.37	~2.42×10^{-6}
BSBN (X=5%)	1.27	~2.09×10^{-6}

cannot explain the change of nominal activation energy. However, the nominal activation energy is a combination of the formation energy of oxygen vacancies (the charge carriers) and the diffusion activation energy. It is possible that the distortion of crystal structure induced by substitution contributes to the increase in the nominal activation energy for the migration of oxygen vacancies.

BIT has a higher remnant polarization than the SBTN system and a similar or even lower coercive field. However, the BIT system suffers from fatigue problem, which may result from bismuth vacancies pinning the dipole switching. Another concern is the multivalence state of Ti ions might contribute to the fatigue problem [27]. Park et al. first reported the partial substitution of A site bismuth (Bi^{3+}) ions with lanthanum (La^{3+}) and claimed excellent fatigue behavior after 10^{10} cycles for $Bi_{3.25}La_{0.75}Ti_4O_{12}$ (BLT) films [46] (see figure 5). Their work suggests that even though bismuth oxide is also very volatile (comparable to lead oxide), suppressing bismuth and oxygen vacancies by partially substituting Bi^{3+} in perovskite-like layers with La^{3+} could greatly improve the reliability behavior since defects in the perovskite-like units are more critical than those in the $(Bi_2O_2)^{2+}$ layers. The fatigue-free properties of the SBTN system also corroborate the hypothesis since bismuth loss is very likely to happen during processing. This further suggests that the influence of multivalence titanium ions in BIT is less significant than bismuth vacancies. Ding et al. used a similar mechanism they proposed in the SBT system [22] to explain the fatigue free property of lanthanum doped BIT: when the lanthanum doping reaches 0.75 (18.75 at%), antiphase boundaries (APBs) start to form while no antiphase domains exist in undoped BIT based on TEM results. These APBs could supply extra nucleation positions for the domain switching process and help make the BLT fatigue free [23]. Besides lanthanum, other rare earth lanthanide ions such as neodymium (Nd^{3+}) and samarium (Sm^{3+}) substitutions for bismuth in BIT are also reported [47-49]. The substituted $Bi_{4-x}Nd_xTi_3O_{12}$ forms a solid solution with up to 50 at% neodymium substitution (x=2). Sol-gel derived thin films of $Bi_{3.54}Nd_{0.46}Ti_3O_{12}$ on a Pt substrate and post-annealed at 700 ° C show high remnant polarization (P_r = 25 $\mu C/cm^2$). Besides larger remnant polarization ($2P_r$ ~ 49 $\mu C/cm^2$), highly *c* oriented $Bi_{3.15}Sm_{0.85}Ti_3O_{12}$ (BSmT) thin film capacitors show little change both in the switching polarization and in the non-switching polarization up to 4.5×10^{10} read/write cycles. This would make BSmT a very promising candidate for nonvolatile memories.

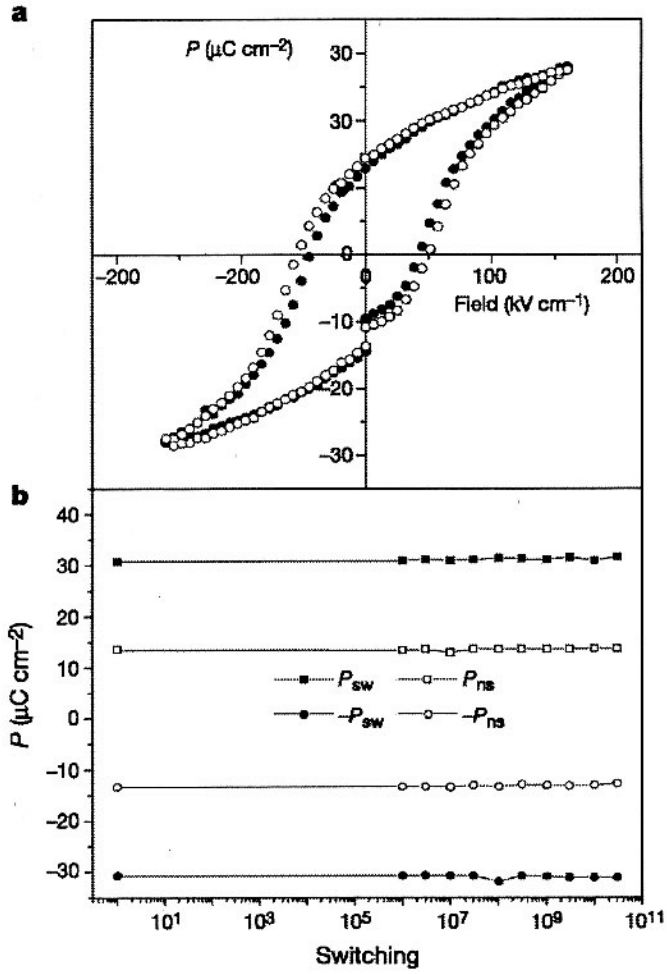

Figure 5. Results of the fatigue tests at 1MHz: P-E hysteresis loops for the Au/BLT/Pt/Ti/SiO_2/Si films before (filled circles) and after (open circles) being subjected to 3 x 10^{10} read/write cycles (a); Variation of P_{sw}, P_{ns}, $-P_{sw}$, and $-P_{ns}$ versus number of cycles (b). The "$-P_{sw}$" and "$-P_{ns}$" denote a switching polarization and linear non-switching polarization, respectively, when a negative read voltage is applied to the capacitor. From T. W. Noh et al. [46]. Reprinted by permission from Nature (Vol 401: 682) copyright (1999) Macmillan Publishers Ltd.

2.1.b. B site ions substitution

Tantalum and niobium ions have the same valence state (+5) and very similar ionic radius (~ 68pm), which might be the reason for formation of continuous solid solution of SBTN system. According to figure 6, with the introduction of niobium ions into SBT, the same layered structure and almost same lattice constants are retained, but both the P_r and E_c values increase [27]. The changes might result from the different electronegativity between tantalum (1.5) and niobium (1.6) [50]. However, how this difference would result in such dramatic change in the niobium/tantalum systems, such as the T_c of $Sr_2Ta_2O_7$ being about 1000 °C lower than that of $Sr_2Nb_2O_7$ [51], still remains unclear. The lower Ec property is possibly the reason that SBT films attracted more interest than SBN. The same good fatigue resistance performance was recorded for SBTN across the entire region of Ta/Nb ratios [27].

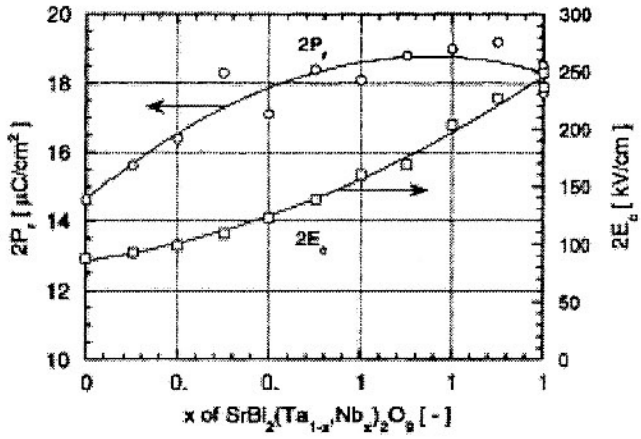

Figure 6. Remnant polarization (represented by $2P_r$) and coercive field ($2E_c$) of the $SrBi_2(Ta_{1-x}, Nb_x)_2O_9$ films. $2P_r$ and $2E_c$ were calculated using hysteresis curves measured at ± 6V. From C. A. P. Araujo et al. [27]. Reprinted by permission from Japanese Journal of Applied Physics.

Vanadium substitution in the SBTN systems proves to be an effective approach for improving the ferroelectric properties of the material [52-57]. Pentavalent vanadium ions have much smaller ionic radius (~58pm) than that of Ta^{5+} or Nb^{5+} (~68pm). Possibly due to its small radius, a full substituted layer structured perovskite compound $SrBi_2V_2O_9$ (SBV) could not be formed [53]. However, the same single-phase layer structure could be kept with vanadium substitution up to ~ 30 at% in SBN. Figure 7 shows the lattice constants change over the various vanadium substitution levels [38]. Both *a* and *c* constants appear to stay more or less constant with small substitution and then decrease linearly when the vanadium content exceeds 15 at%. The changes were explained by

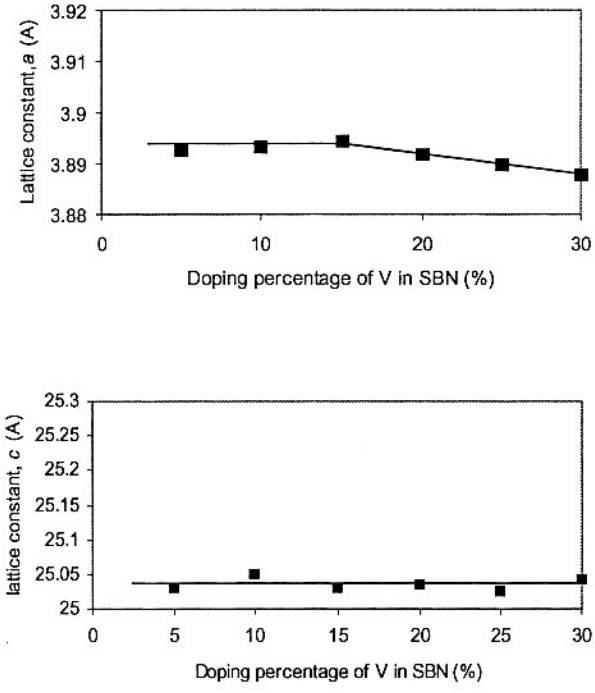

Figure 7. Lattice constant change over vanadium doping content.

smaller ionic radius of vanadium and the constraint effect from the bismuth oxide layers. Although the lattice constants tend to shrink with smaller center ions substituted in perovskite like units, the bismuth oxide layers tend to prevent the shrinkage until a critical doping concentration is reached. With vanadium substitution, the sintering temperature of SBTN ceramic system was found to be lowered ~200-300 °C, as vanadium oxide has a low melting point, which also explains the fact that vanadium oxide is commonly used as sintering aid for lower temperature sintering ceramics [58-59]. More importantly, the dielectric and ferroelectric properties were significantly enhanced by vanadium substitution. Figure 8 shows the dielectric constants of $SrBi_2(V_xNb_{1-x})_2O_9$ (SBVN, x = 0-0.3) as a function of temperature at a frequency of 100 kHz. The Curie temperature increases almost monotonically with the increasing vanadium content (see figure 9). Around 10 to 15 at% of vanadium substitution, the maximum dielectric constant value ε_{max} is about 40 % higher than that of undoped SBN. Further, the P-E hystereses of SBVN were measured at 178 °C for SBN and 150 °C for

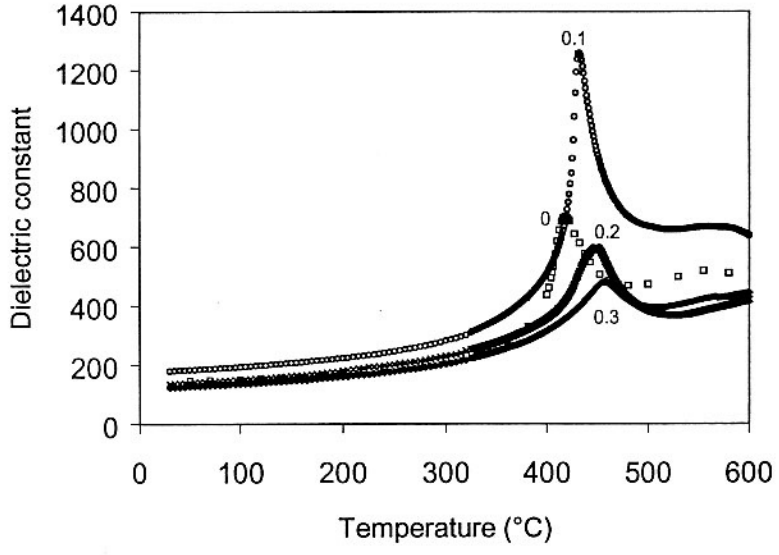

Figure 8. Dielectric constant measured at 100 kHz versus temperature for various vanadium doping content in SBN.

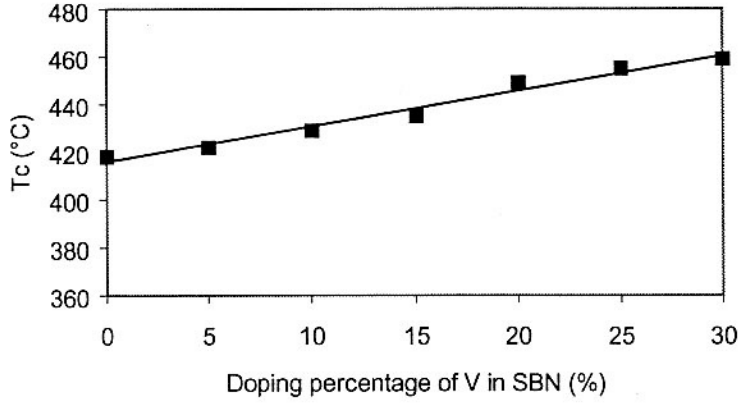

Figure 9. Curie temperature vs. vanadium substitution content in SBN.

the two SBVN samples with a Sawyer-Tower circuit at 10 Hz (Figure 10). Table 2 summarizes the peak dielectric constants, P_r, E_c values of SBVN system. With ~ 10 at% vanadium substitution, the P_r of SBN increases from ~ 2.8 to ~ 8 $\mu C/cm^2$ while the coercive field E_c value decreases from ~ 63 to ~ 50 kV/cm. Combined with the low sintering temperature, SBVN could be a very promising candidate for future high-density FeRAM devices. As discussed above, the lattice constants do not change much with up to 15 at% vanadium substitution, the "rattling space" of center ions could be significantly enlarged with much smaller vanadium ions. Higher T_c values also suggest that the stability and polarizability of SBN is strengthened by vanadium doping. The smaller coercive field might also be due to the substitution with smaller ions making the switch of polarization easier. Similar with CSBN and BSBN, SBVN ferroelectrics also show lowered dc conductivity than that of SBN (see figure 11). Vanadium substituted SBT, $SrBi_2(V, Ta)_2O_9$ (SBVT) films with deficient strontium and extra bismuth were also reported [60]. With partial substitution of vanadium for tantalum around 7.5 at%, the remnant polarizations ($2P_r$) of $Sr_{0.8}Bi_{2.3}Ta_{1.85}V_{0.15}O_9$, SBVT films annealed at 800 °C increased to ~ 30.5 $\mu C/cm^2$ from ~ 18.1 $\mu C/cm^2$ for Sr-deficient SBT films. Such a significant enhancement of remnant polarization is attributed mainly to the enlarged

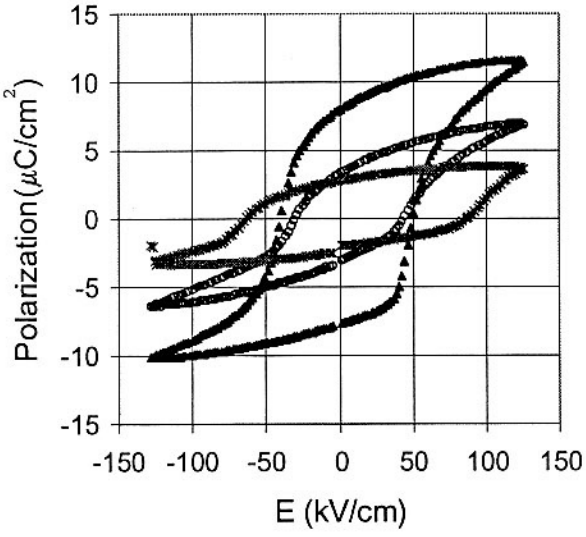

Figure 10. P-E hysteresis curves for SBN (*, at 178 °C), with 5 at% vanadium (○, at 165 °C) and with 10 at% vanadium (□, at 165 °C).

Table 2. The peak dielectric constants, P_r, E_c values of SBVN system. X stands for the atomic percentage of substituting ions V^{5+} in SBN.

Sample	ε_{max} (100kHz)	P_r ($\mu C/cm^2$)	E_c (kV/cm)
SBVN (X=0)	~ 700	3	63
SBVN (X=5%)	~ 1140	3.5	40
SBVN (X=10%)	~ 1040	8	50

"rattling space" due to the substitution by smaller vanadium ions. Similarly, with SBVT ceramics [57], the leakage current density of Sr-deficient SBT films were appreciably reduced with vanadium substitution up to ~ 7.5 at%. Further, the incorporation of a limited amount of vanadium into the layered structure was found to have no noticeable influence on the fatigue resistance of Sr-deficient SBT (see figure 12). Besides the SBTN system, enhanced dielectric and ferroelectric properties of $BaBi_4Ti_4O_{15}$ (BBT) single crystal is also reported with partial substitution of titanium by vanadium [61].

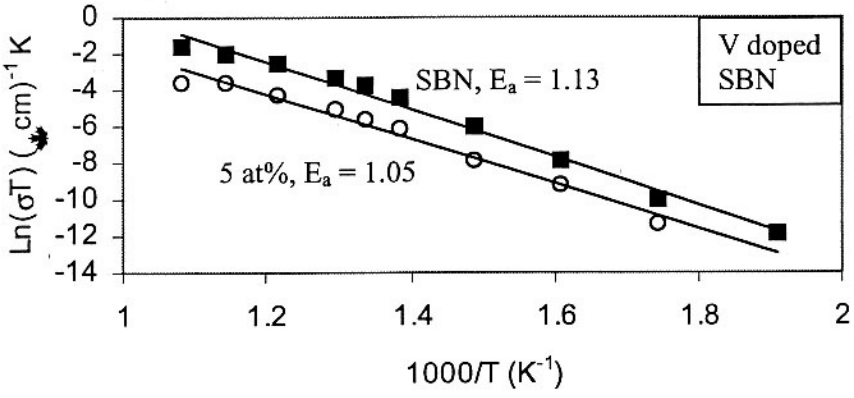

Figure 11. DC conductivity of 5 at% vanadium substituted SBN ceramics.

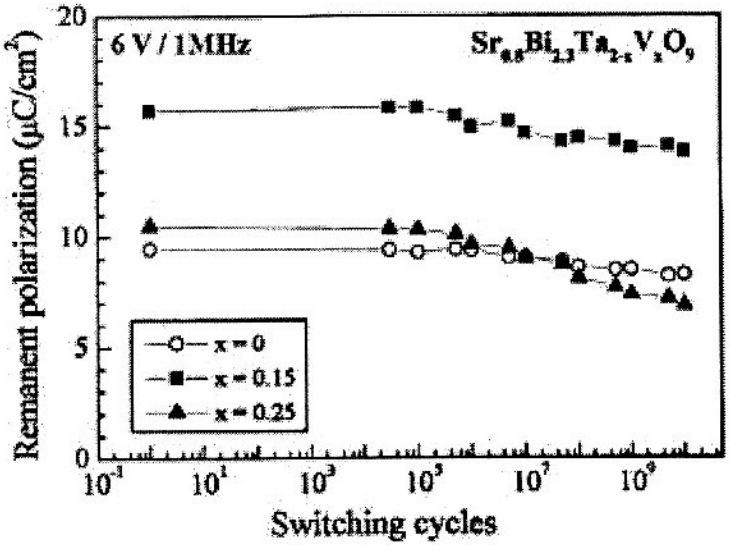

Figure 12. Fatigue behavior of $Sr_{0.8}Bi_{2.3}(Ta_{2-x}V_x)O_9$ films with an applied voltage of 6V at 1 MHz. From Chen et al. [60]. Reprint permission from Journal of Applied Physics.

2.2. Different valence ions doping

2.2.a. A site ions doping

One widely reported advancement in improving SBTN system properties is to have a strontium deficiency compensated with excess bismuth [62]. Bi^{3+} ions is used as

dopants for A site ions Sr^{2+} since they have similar ionic radii, ~131pm for Bi^{3+} and ~140pm for Sr^{2+} [41]. The doping of bismuth on strontium site favors the center ions displacement [63], which might account for the remnant polarization enhancement in SBTN films with a strontium deficiency and excess bismuth (see figure 13). This doping effect also results in a higher T_c in the SBT system, which implies improved stability and polarizability of the perovskite structure [64]. Ding et al. studied this effect from the microstructure point of view. In their work, it cannot be confirmed that the excess Bi substitutes for Sr in the whole structure to enhance the distortion in TaO_6 octahedra, leading to the larger ferroelectric polarization. However, it is confirmed from their TEM results that the excess Bi and the deficient Sr can decrease the stacking fault density and control the form of the stacking faults, which could account for the improvement of ferroelectric properties [65].

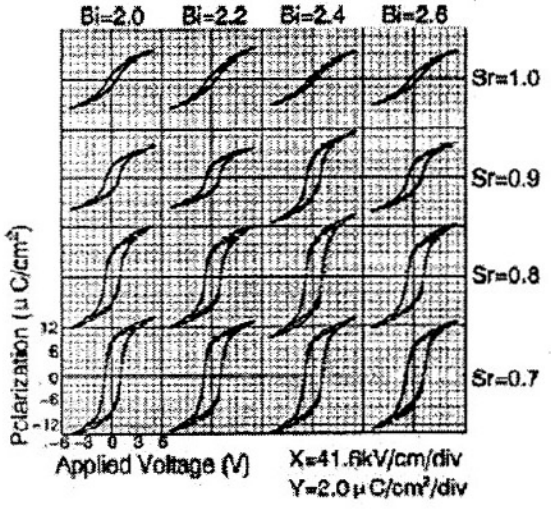

Figure 13. P-E hysteresis curves of SBT (x/y/2.0)/Pt/Ti films. From Atsuki et al. [62]. Reprint permission from Journal of Applied Physics.

A disadvantage of SBTN with Sr deficiency and excess bismuth is possible degradation of fatigue resistance (~ 10% loss after 10^{10} cycles in $Sr_{0.8}Bi_{2.3}Ta_2O_9$ films [60]), while stoichiometric SBTN films show excellent fatigue properties [66]. However, there is also a report showing that $Sr_{0.7}Bi_{2.3}Ta_2O_9$ films annealed at 700 °C or 800 °C had no appreciable P_r changes after 10^{11} cycles [67]. Excess bismuth is also reported to be effective in promoting the fluorite phase to the bismuth layer structure [68]. The comparison between the films with $Sr_{0.7}Bi_{2.0}Ta_2O_9$ and $Sr_{0.7}Bi_{2.8}Ta_2O_9$ suggests that too much bismuth might degrade the film leakage resistance [69]. A possible explanation is that bismuth might accumulate at grain boundaries in the form of bismuth oxide or even metallic bismuth (especially after reductive environment annealing), which makes the film quite leaky.

2.2.b. B site ions doping

Cations with a higher valence state were also exploited to dope in the B sites of SBN crystal. For example, SBN ceramics doped with tungsten oxide, with a composition of

Sr_{1+x} $Bi_{2-4/3x}(W_x$ $Nb_{1-x})_2O_9$, with x ranging from 0 to 0.2 (20 at%) were prepared by solid-state reaction sintering [70]. Compared to Nb^{5+} (~69 pm), W^{6+} has higher valence state and smaller ionic radius (~64 pm) at the same coordination number (CN) of 6. XRD spectra show that single phase layered perovskites were formed when the doping content of tungsten was below 2.5 at%, but some extra peaks appear in samples consisting of more than 5 at.% tungsten, indicating possible formation of unknown secondary phase(s). Compared to vanadium substitution (single phase being kept at least up to ~30 at% [52]), tungsten has a much lower solubility in SBN, though the ionic radius of tungsten ions is closer to that of pentavalent niobium ions than that of pentavalent vanadium ions. It is not known why tungsten has a lower solubility, but it is possible that the higher valence state (6+) of tungsten will influence the stability of the crystal structure of SBN ferroelectrics. Fig. 14 shows the dielectric constants as a function of temperature for SBWN ceramics consisting of 0, 1, 2.5 and 10 at.% tungsten, determined at a frequency of 100 kHz. It is clear that tungsten doping resulted in increased peak dielectric constants and lowered Curie points.

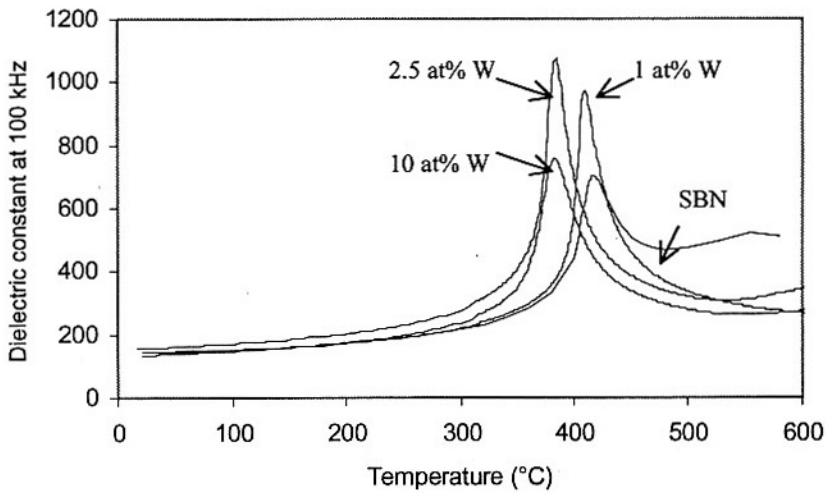

Figure 14. Dielectric constant measured at 100 kHz versus temperature for various tungsten doping content in SBN.

Table 3 summarizes the P-E hysteresis results of the SBWN samples measured at room temperature with x = 0, 0.025, and 0.1 respectively. The remnant polarization increases significantly from approximately $2P_r = (P_{r+} - P_{r-}) = 4.4$ μC/cm^2 for SBN to $2P_r$ = 12.6 μC/cm^2 for 2.5 at% doped SBWN, and to $2P_r$ = 60 μC/cm^2 for 10 at % doped SBWN. The coercive field, $2E_c$, first remains at ~160 kV/cm for SBWN up to 2.5 at% tungsten, and then increases to ~240 kV/cm with 10 at% tungsten doping (Figure 15).

The polarization could be analyzed by the relation [71]:

$$P_x = \sum_i (q_i \Delta x_i) V^{-1} \tag{3}$$

where P_x is polarization, q is the electrical charge of the centering cation, Δx is the displacement of the center ion, and V is the unit cell volume. Larger electrical charge (q)

Table 3. P-E hysteresis results of the SBWN samples measured at room temperature. X stands for the atomic percentage of doping ions W^{6+} in SBN.

Sample	P_r ($\mu C/cm^2$)	E_c (kV/cm)
SBWN (X=0)	2.2	80
SBWN (X=2.5%)	6.3	80
SBWN (X=10%)	30	120

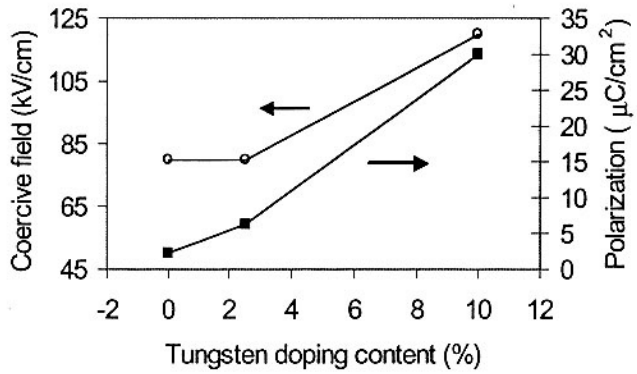

Figure 15. Remnant polarizations and coercive fields of $Sr_{1+x}Bi_{2-2/3x}(WxNb_{1-x})_2O_9$ ferroelectric ceramics.

and/or larger charge displacement (Δx) would result in larger polarization, assuming the same cell volume. In the SBWN system, XRD results indicated that there was no noticeable shift of XRD peaks with tungsten doping, suggesting no appreciable change in the lattice constant of the SBN perovskite crystal. Therefore, the size difference and the valence difference of tungsten and niobium ions would play important roles. The higher ionic charge of W^{6+} would contribute to the increase of ferroelectric polarization. Since W^{6+} has a smaller ionic radius, it may also have the similar effect as enlarging "rattling space" to SBN system. However, according to the dielectric properties measurement, an increased amount of tungsten doping resulted in a reduced Curie temperature, which implied decreased stability of the perovskite structure. The decrease of Tc suggests that the higher dielectric constant peak and P_r may not be due to higher polarizability, which happens in vanadium substitution through increased "rattling space" inside the oxygen octahedra. The higher valence state of tungsten might have a stronger influence on polarization than its size. The increased coercive field may be due to the high valence state of tungsten ions, which may contribute to an increased barrier for dipole switching. In general, the substitution of alternative cations in isotropic perovskite ferroelectrics would have the effect of restricting domain wall motion, and thus result in an increased coercive field [41]. It is possible that small amount of tungsten cations (2.5 at%) did not significantly change the potential energy to rattle from one position to another inside the oxygen octahedron. However, with higher doping

content (10 at%), the higher ionic charge effect might be dominant and lead to the sharp increase of the coercive field. Figure 16 shows that after tungsten doping, the DC conductivity decreases significantly compared to the SBN. Similar with other doping systems, the activation energies of tungsten-doped sample are also higher than undoped SBN samples. It is not clear what the exact mechanism is for the reduction of DC conductivity with tungsten doping. Although the weaker W-O (~ 672 kJ/mol) [45] chemical bond compared with that of the Nb-O bond (~703 kJ/mol) [45] permits easier formation of oxygen vacancies the higher valence state of W^{6+} may effectively suppress the formation of oxygen vacancies and, thus, reduces the electrical conductivity.

Vanadium and tungsten doping in BIT have very similar results as to those in SBTN. Lanthanum substituted BIT ($Bi_{3.25}La_{0.75}Ti_3O_{12}$) improves fatigue properties of BIT but lowers the T_c and increases the E_c. Another way to enhance the intrinsic ferroelectric properties in BIT is to dope higher valence cations on Ti^{4+} sites in perovskite units. Noguchi et al. reported to have enhanced P_r values up to ~ 20 $\mu C/cm^2$ in BIT through vanadium and tungsten doping [72]. Higher valence ions (V^{5+} or W^{6+}) doped into BIT is believed to suppress the formation of oxygen vacancies, and result in a significant decrease in V_{Bi}'''-$V_O^{\cdot\cdot}$ complexes which are believed to act as effective pinning sites in BIT [72].

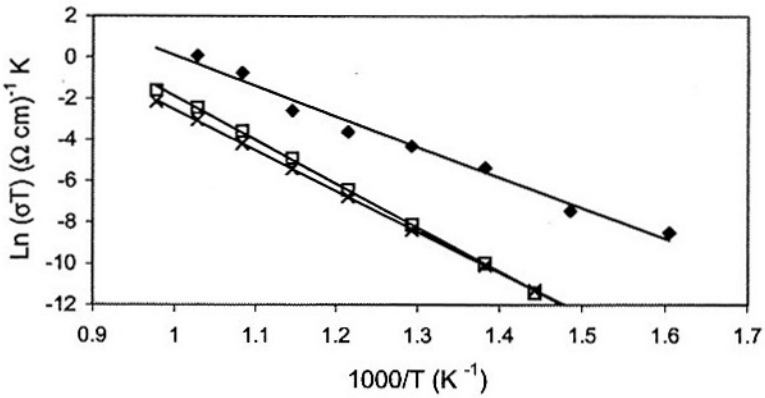

Figure 16. DC conductivity versus temperature: ♦ (SBN); (2.5 at% SBWN); × (10at% SBWN).

2.2.c. ABO_3 type doping

To further improve dielectric and especially piezoelectric properties, doping effects were exploited in some more complex isotropic systems, such as $Pb(Mg, Nb)O_3$ (PMN)-$PbTiO_3$ (PT), $PbTiO_3$ (PT)-$BiFeO_3$ and $BaTiO_3$-$BiFeO_3$ etc [73-75]. Ko et al. proposed a series of BLSF-nABO_3 to adjust the perovskite units of BIT system. $Bi4Ti_3O_4$-$BiFeO_3$ was formed to add one extra perovskite slab between the $(Bi_2O_2)^{2+}$ layers. As a result, the *c* axis of BIT expands and the oxygen octahedra in the perovskite layers becomes less constrained by the bismuth oxide layers [76]. With a small doping content, the original single phase BLSF structure (including the number, m) could be retained. $BiFeO_3$-SBN with Fe^{3+} doping for Nb^{5+} was reported to have significant enhancement of dielectric properties with a composition of 0.3$BiFeO_3$-0.7SBN [77]. The single phase of layered structure could be formed with the composition as x$BiFeO_3$-(1-x)SBN (SBFN, x ranging from 0 to 0.3). The Curie points of SBFN shift to higher values with a high $BiFeO_3$ content. 0.3$BiFeO_3$-0.7SBN exhibits a maximal dielectric constant of ~ 1.84 x 10^5

at its Curie point of ~ 750 °C measured at 10 kHz. Considering the similar lattice dimensions to SBN, the extremely large dielectric constant of $0.3BiFeO_3$-0.7SBN may be attributed to the enlarged rattling space by the introduction of smaller ions, Fe^{3+}. In addition, the addition of $BiFeO_3$ improves the sinterability of SBN ceramics.

Bi_2SiO_5 (BSO) has also been studied for its doping effect in BLSFs. Although BSO does not belong to ABO_3 type compounds, it possesses a bismuth layer structure with a crystallization temperature as low as 400 °C [78]. Kojima et al. reported BSO doping in BIT, SBT and PZT films by sol gel processing [79]. With doping of BSO, the mixture films were crystallized at 500 °C. The high temperature XRD results show that at 400 °C there are only BSO phase crystallization peaks and at 500 °C both phases appear. When temperature reduces to room temperature, the BSO peaks disappear and only BIT peaks remain. This suggests that BSO phase transforms to bismuth layer perovskite during cooling and a single phase, silicon doped $Bi_4(Ti, Si)_3O_{12}$, is formed. XPS results also show that the Si 2p state in BSO-BIT film shifts up about 1.5 eV, suggesting that the coordination number of most Si increases from 4 to 6 to form SiO_6 octahedra. However, it was generally known that the Si-substituted crystals with perovskite structure are found only in the mantle of the earth because the ionic radius of silicon is too small to form a perovskite structure at atmospheric pressure [80]. This proposed phase transition is further attributed to the huge stress generated by the thermal expansion difference between BSO and BIT during cooling, which is high enough to form the SiO_6 octahedral structure. With doping of BSO, BIT films keep the same square shaped P-E loop and P_r values as pure BIT, but with fatigue free properties up to at least 10^{10} switching cycles as compared with up to ~10^8 cycles of undoped BIT films [81]. In addition, the films show very little degradation after annealing in N_2 atmosphere with 3 % H2 at 400 °C for 10 min, which is a significant improvement on hydrogen immunity for BIT system (see figure 17). Further, it was found that BSO is effective in improving the surface morphology and in lowering the crystallization temperature of SBT and PZT films.

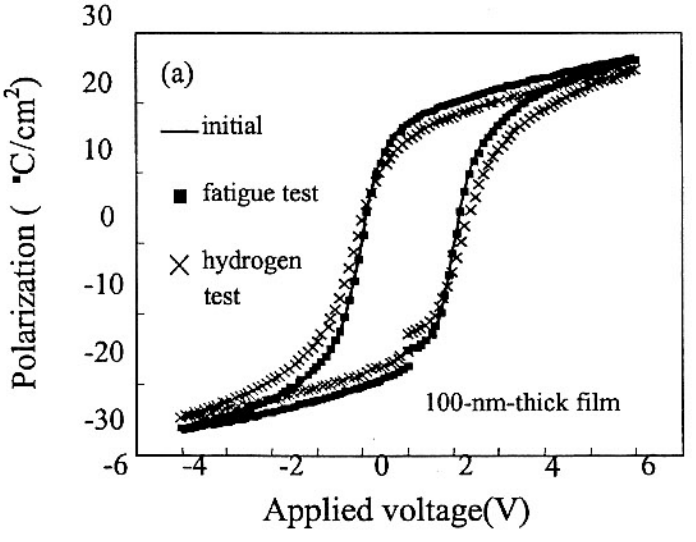

Figure 17. Variation of P-V hysteresis curves of a BSO-BIT capacitor. Solid line for initial and closed squares for after fatigue test of 10^{10} switching cycles at 100 kHz; cross for after hydrogen immunity test at 400 °C. From Ishiwara et al. [79]. Reprinted by permission from Japanese Journal of Applied Physics.

2.2.d. $[Bi_2O_2]^{2+}$ layer doping

The Bi_2O_2 sheets in layer structured perovskites were considered unalterable [25]. Millan et al. reported the substitution of Bi^{3+} in $[Bi_2O_2]^{2+}$ layers by cations such as Pb^{2+}, Sb^{3+}, Sn^{2+} or Te^{4+} [71,82-83]. They first tried to dope Pb^{2+} into Bi_2O_2 layer of SBN because Pb^{2+} has similar ionic size and same $6s^2$ lone pair electrons as Bi^{3+}. Through solid-state reaction, it was demonstrated that not only is the substitution into Bi_2O_2 layer possible without destroying the basic crystal structure, but also the entire $SrBi_{2-x}Pb_xNb_2O_{9-x/2}$ ($0 \leq x \leq 2$) solid solution could be formed. The introduction of larger Pb^{2+} into Bi_2O_2 sheets of SBN leads to a monoclinic distortion, probably due to the presence of oxygen vacancies in order to retain the charge neutrality. Smaller Sb^{3+} and Sn^{2+} were also able to replace Bi^{3+} in SBN, forming single phase $SrBi_{2-x}Sb_xNb_2O_9$ and $SrBi_{2-x}Sn_xNb_2O_{9-x/2}$ ($0 \leq x \leq 1$). Both Sb^{3+} and Sn^{2+} have the same $5s^2$ lone pair of electrons, which might lead to the same amount of doping limit into SBN. When doped more than 50 at%, a second phase starts to appear. This might be due to possible lattice mismatch strain generated by the rearrangement of the $(Bi, Sb)_2O_2$ or $(Bi, Sn)_2O_2$. Possessing same $5s^2$ lone pair electrons, Te^{4+} can also be doped into the Bi_2O_2 layer of SBN. To keep the charge neutrality, the lower valence ions sodium or potassium were co-doped into A site for strontium. These dopings cause the appearance of additional peaks in the dielectric constant versus temperature curve and lower Tc values [71].

3. Microstructure adjustment

3.1. Orientation engineering

The inherent layered structures of SBTN and BIT naturally result in strong anisotropic properties, such as polarization and conductivity. The spontaneous polarization along the *c*-axis is blocked by the bismuth oxide layers, so the spontaneous polarization (P_s) vector lies within or very close to *a-b* plane. According to Newnham et al., there would be no Ps along the *c* axis when there are an even number of perovskite units between the bismuth oxide $(Bi_2O_2)^{2+}$ layers, which is attributed to the mirror symmetry, so that the spontaneous polarization of the individual BO_6 octahedra cancels each other out [25]. This probably explains that for the SBTN system with m = 2, *c*-oriented films were reported to have shown no or little remnant polarization [84]. Because of this anisotropy, the randomly oriented Sr-deficient SBN films have larger remnant polarization than *c*-axis oriented stoichiometric SBN films [85]. Desu et al. reported that they got preferable results (reasonably large P_r with small E_c) in c-oriented SBN film deposited on (111) Pt electrodes [86]. This suggests that the P_s vector in SBTN might not be strictly perpendicular to the *c* axis. Through sol gel processing, Wu et al. also made *c* oriented SBN films on (100) $SrTiO_3$ single crystal substrates [87]. Besides *c* orientation, (116) and (103) oriented SBT films could be grown on buffered silicon (100) substrates [88]. Bi_3TaO_7 was reported to be an effective seed layer in obtaining *a* (or *b*) oriented SBT films that have higher remnant polarizations [89]. Varying the Sr source is reported to be effective in controlling the *c* or *a*(*b*) orientation in $Sr_{0.7}Bi_{2.3}Ta_2O_9$ films prepared by chemical solution deposition (CSD) [90].

BIT films made by MOCVD have the tendency to be *c*-axis oriented [91]. Extra amounts of bismuth were reported to be helpful in obtaining *c*-oriented BIT films. Another report of *c*-axis oriented BIT films on platinized silicon substrate was made by first spin-coating with a 10 at% Bi-rich solution and annealing at 800 °C to get a highly *c*-axis oriented seed BIT film. On this seed layer, BIT films spin-coated using stoichiometric solution show high *c*-axis orientation and extremely flat surface [92]. Through adjusting baking conditions, lanthanum substituted BIT films with (117) and (001) orientations are prepared by CSD on $Pt/TiO_2/SiO_2/Si(100)$ substrates [93]. Low P_r and E_c values were obtained for *c*-oriented BIT films. Such morphology and properties make *c*-oriented films preferable choice for fabrication of Metal - Ferroelectrics - Insulator -Semiconductor (MFIS) structures or devices because the coercive field is very small. It is interesting to note that *c*-oriented films of SBTN and BIT both show not only smaller P_r but also smaller E_c. Smaller P_r is due to the polarization vector direction and the smaller E_c might come from pure 180 degree domain walls, which result in no internal stress during domain motion.

3.2. Grain size effect

Yamaguchi et al. reported that *c*-oriented BIT films with small grain size show superior properties over large grain sized films: larger P_r, lower leakage current, higher break down strength, etc. [94]. Films annealed at high temperature (large grain size) have decreased *c*-axis lattice constants, with better crystallinity [95]. The lattice change was attributed to the smaller thermal expansion coefficient of silicon than that of BIT. It was postulated that the lattice constants shrank more along the *c*-axis than along the *a*-axis [95]. This suggests that the decreased P_r might be due to smaller displacement along the *c*-direction. For very thin films (~ 100 nm thick or less), smaller grains tend to be favorable due to lower leakage current and better reliability [18]. High breakdown voltage of thin films with fine grains could be due to the homogeneous microstructure with small sized defects. However, the films with large grains have better crystallinity and, thus, produce better P-E hysteresis. One model for thin ferroelectric films size effect is the domain structure transition from multi-domain predominance to single domain predominance when the grain size shrinks to a critical value [96]. The single-domain predominated grain is very stable under an external field, which would make the domain nucleation quite difficult and lower down the domain wall mobility. For example, SBVT films have higher P_r with 800 °C annealing as compared to 700 °C annealing [60]. Sr-deficient SBT, $Sr_xBi_{2z}Ta_2O_9$ (0.7□x□1.0, 2.0□2z□2.6), films show enhanced P_r with a decreased strontium content, which is also explained by increased grain size [62]. Aizawa et al. reported that SBT films annealed by a face-to-face setup (two film samples, one covering another with the pre-dried film sides sticking together during final annealing) also showed enhanced ferroelectric properties due to large grains [97]. Zhu et al. further pointed out that the size effect of BLSFs thin films ($0.8SBT\text{-}0.2Bi_3TiNbO_9$) was mainly determined by the grain size instead of the thickness in the range of 80-500 nm since the large difference between the lattice constants of *a* and *c* in the BLSFs causes anisotropic grain growth and the grain growth is not limited by the film thickness. [98]. However, large grained SBT films may be obtained with inferior performances also due to the interface effects after processing at high temperatures. It is reported that the

higher substrate temperature in pulsed laser deposition of SBT films was used to induce grain growth. However, the topology of the top electrode (Al) and the interface between SBT and SiO_2 becomes rough [69] and this roughening increases the local electric field and results in high leakage current in the SBT films.

In bulk ceramics, the grain size effect on dielectric properties in SBN and SBVN were also studied [99]. It was found that generally the large grained samples yield high maximal dielectric constants (ε_{max}) at Curie temperatures, in which the large grain size was achieved by prolonged sintering up to 10 hours. However, samples with further extended sintering up to ~ 20hrs show lower ε_{max} with even larger grain size (figure 18). Bismuth-layered compounds such as $Bi_2VO_{5.5}$ (BIV), Bi_3TiNbO_9 (BTN) and BIT show increased dielectric constants with either increased grain size [100] or film thickness [101]. It was suggested that these materials contain a thin layer of a Bi-rich and low dielectric constant substance at grain boundaries. For large grained films, the thickness of grain boundary layers has been observed to decrease, along with a corresponding decrease in the total volume of grain boundary phase. This gives a large value of the dielectric constant as the grains increase in size. A similar mechanism likely causes the dielectric constants of SBN and SBVN to increase with sintering time increases up to 10 hours.

Lattice defects are known to affect the dielectric constant through the suppression of domain formation [102]. Thus, the dielectric constant decreases as the number of defects increases. This is another possible explanation for the increase in dielectric constant with increasing sintering times up to 10 hours, as lattice defects are removed during prolonged annealing. However, it is not clear why the extended sintering (20 hrs) would decrease the ε_{max} values in SBN and SBVN ceramics. One possible explanation is that more oxygen vacancies were generated by Bi_2O_3 loss during prolonged sintering. This also suggests that although grain size is an important factor affecting dielectric properties of BLSFs, other factors such as defects and chemistry (e.g. change of valence state) should also be taken into consideration.

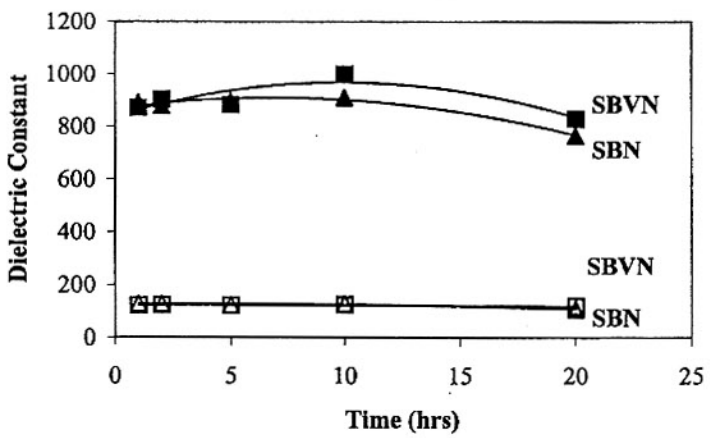

Figure 18. Dielectric constants verses sintering time for both SBN and SBVN samples, measured at a frequency of 100 kHz. Included in this figure are both the peak and room temperature values.

4. Annealing

Annealing is very important in the preparation of BLSFs. In principle, there are two annealing processes. One is referred to as pre-annealing, which is to remove residual

organic species by heating the samples to elevated temperatures, but lower than sintering temperatures, prior to sintering. Another is post-annealing after sintering to further improve the crystallinity, release possible stress and remove oxygen vacancies.

4.1. Pre-annealing in sol-gel coating

Carbon residues are known to play an important role in crystallization process of films made by sol-gel processing and chemical solution deposition (CSD). Low carbon contents in the films can be easily removed through oxidation and benefit the crystallization of the films. Ma et al. reported garnet films of $Bi_1Dy_2Fe_5O_{12}$ (BDF) prepared using a so-called modified Pechini process, in which ethylene diamine tetraacetic acid (EDTA) rather than citric acid (CA) acted as a chelating agent. The results of analysis on crystallization characteristics of derived BDF films showed that efficient removal of organic compounds and carbon residuals by pre-annealing before the firing process was vital to the formation of a single-phase crystalline garnet [103]. This process is also found effective in the preparation of BLSFs films. SBT films were reported with better dielectric and ferroelectric properties using alkoxides as precursors whose carbon number in each organic ligand is 4 or less [68]. Usually the thermal gravity (TG) curve could be used to determine the pre-annealing temperature. The pre-annealing temperature should be higher than the temperature at which weight loss more or less stops, which suggests the removal of organic compound and carbon residues. Besides temperature, the pre-annealing atmosphere is also important in getting rid of carbon residues during the preparation of BLSF films. SBT films prepared by CSD first calcined at a low oxygen partial pressure in a mixture of N_2/O_2 and then crystallized in N_2 did not form the SBT phase structure. Thermal desorption mass spectrometry (TDS) shows that the carbon content of the film calcined in deficient O_2 is higher than that calcined in rich O_2 [104].

4.2. Post-annealing effect

Similar to pre-annealing, atmosphere could play an important role in the post-annealing. The influences of three types of annealing atmospheres on BLSF films were reported, such as oxidizing (air or O_2), reducing (H_2) and neutral (Ar or N_2), though annealing in air or oxygen is most widely reported. Kodama et al. shows that 600 °C annealing in O_2 atmosphere after deposition of SBT film could improve the retention characteristics of MFIS structures [105]. It was revealed that the O_2 annealing could reduce the surface roughness of the SBT film. The annealing improves crystallinity of the films and decreases the oxygen vacancies in SBT, and thus leads to fewer traps and lower space charge density [105]. Annealing in O_2 gas at a high pressure is also reported to be effective for the formation of *c*-axis oriented BIT films with a smooth surface and improved electrical properties [106]. In contrast to annealing at ambient oxygen, degradation of electrical properties by annealing in ambient hydrogen remains a big challenge for the integration of FeRAMs [107]. The bismuth oxide in SBT films could be reduced to metallic bismuth by H_2 annealing and leads to high leakage current [108]. Hydrogen annealing may result in more serious degradation in properties of BIT than SBTN since BIT has more bismuth sites. The second annealing at 800 °C in O_2

atmosphere (after H_2 annealing) could lower the leakage current of SBT films by oxidizing the metallic Bi and reducing the oxygen vacancies. Similar with hydrogen annealing, structural and compositional analyses suggest that some Bi atoms in the SBT films become free of oxygen due to annealing in argon gas for short periods at 700 °C. After argon annealing, a second annealing (oxygen) also at 700 °C yields similar structure with 800 °C annealed SBT films [109].

Besides the films, post annealing also has an appreciable influence on the electrical properties of bulk BLSF ceramics. The influences of O_2 and N_2 annealing on the dielectric properties of SBVN ferroelectrics were studied [110]. After sintering at 950 °C for 2 hrs in air, samples were annealed at 800 °C for 3 hrs in O_2 or N_2. With O_2 annealing, the Curie point of the SBVN ferroelectrics shifted to higher temperatures and the peak dielectric constant increased more than 30 % (figure 19). However, no change in the Curie point was found with N_2 annealing. Furthermore, O_2 annealing was found to reduce significantly both the dielectric constant and loss tangent of the SBVN ferroelectrics at frequencies below 1000 Hz at room temperature. Figures 20 and 21 are the dielectric constant and tangent loss of SBVN ferroelectrics as functions of frequency, ranging from 20 Hz to 1 MHz at room temperature. Change of dielectric constants and tangent loss is attributed to the change in the valence states of vanadium ions in SBVN ceramics when subjected to O_2 and N_2 annealing. The experimental results imply that some V^{4+} ions, which are compensated by the formation of oxygen vacancies, existed in the SBVN ferroelectrics prior to O_2 annealing. When V^{4+} are incorporated into the SBVN layered perovskite structure by substituting Nb^{5+}, oxygen vacancies would be created. Using Kroger-Vink notation:

$$2VO_2 = 2V_{Nb}' + 4O_O + V_O^{\cdot\cdot} \quad (4)$$

where V_{Nb}' represents V^{4+} occupied Nb^{5+} site with one effective negative charge and $VO^{\cdot\cdot}$ represents an oxygen vacancy with two effective positive charges. Both V_{Nb}' and $VO^{\cdot\cdot}$ are potential charge carriers, and possible contributors to space-charge polarization.

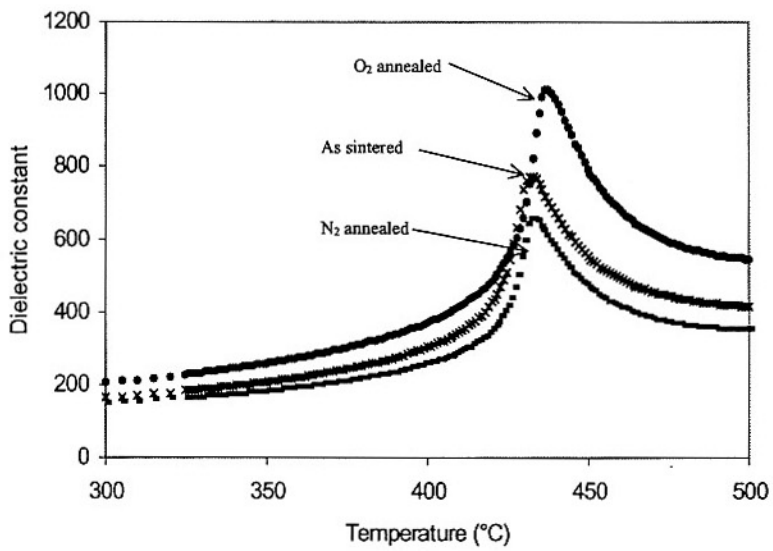

Figure 19. Temperature dependence of dielectric constants of SBVN samples with O_2 annealing, without annealing and with N_2 annealing measured at 100 kHz .

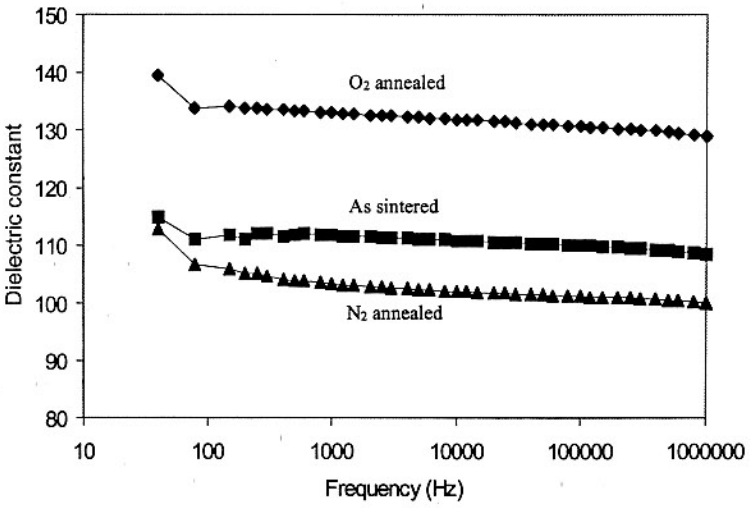

Figure 20. The dielectric constants of SBVN samples versus frequency at room temperature.

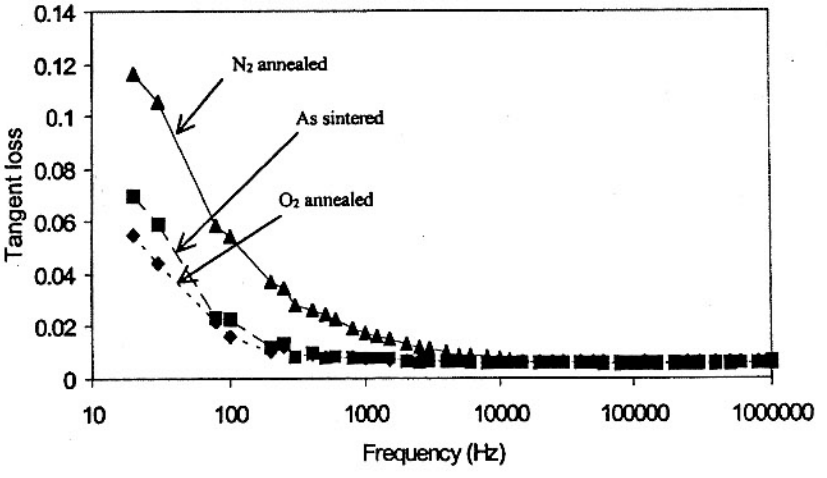

Figure 21. The tangent loss of SBVN samples versus frequency at room temperature.

V^{4+} ions could be oxidized to V^{5+} with O_2 annealing, which resulted in improved dielectric properties. However, due to the low concentration of vanadium ions, XPS analyses did not produce any direct evidence supporting or refuting this possible explanation, particularly those with a tetravalent state.

Post-annealing temperature has a noticeable influence on dielectric and ferroelectric properties. When the annealing temperature was very low, the $Sr_{0.7}Bi_{2.3}Ta_2O_9$ films prepared by CLD showed no spontaneous polarization after annealing at 650 °C, and ferroelectric properties were obtained only when the films were annealed higher than 700 °C [111]. The squareness of the P-E loops (ratio of remnant polarization over saturation polarization, P_r/P_s) was further improved after the samples were annealed at 800 °C. The difference in the samples annealed at different temperatures was attributed to the crystallinity and crystal grain size confirmed by microscopy. In the mean time, too high post annealing temperature may induce more oxygen vacancies in the films. Shi-Zhao et al. reported the variations in the level of ferroelectric fatigue of $Sr_{1-x}Bi_{2+y}Ta_2O_9$ thin-film capacitors with Pt electrodes as a function of the heat-treatment temperature

[112]. The ~220 nm SBT thin films were spin coated on $Pt/TiO_2/SiO_2/Si$ substrate and crystallized at 800 °C. The post-annealing temperature varied from 800 to 950 °C was found to barely affect P-E hysteresis results. However, the samples annealed at 900 and 950 °C showed serious ferroelectric fatigue after ~10^8-10^9 switching cycles, whereas the sample annealed at 800 °C showed fatigue-free behavior up to 10^{10} cycles. This behavior appeared to have a close relationship with the loss of oxygen from the SBT layer during high temperature annealing.

Furthermore, not only the amount of vacancies but also their distributions could have essential influences on ferroelectric properties. Therefore, the post annealing at temperatures above T_c could be used to redistribute the existing vacancies in the system. Noguchi et al. found that quenching might help keep the random distribution of the vacancies and thus improve the electrical properties of the BIT [72]. Tan et al. reported that the vacancies accumulated near domain boundaries could cause domain pinning, and thus reduce P_r of the potassium doped PZT samples [113]. The influence of domain pinning could be reduced by the random distribution of vacancies.

5. Summary

With appropriate doping or substitution, electrical, dielectric and ferroelectric properties of layer structured perovskite ferroelectrics can be significantly enhanced or modified. It was further demonstrated that the properties are strongly dependent on the grain size, preferential crystal orientation, and annealing conditions.

References

1. Jona, F. and Shirane, G. 1962, Ferroelectric Crystals, Pergamon Press, New York.
2. Cao, G. Z. 2001, Ferroelectrics and Applications; pp. 86-112 in Advances in Materials Science and Applications. Edited by D. L. Shi. Tsinghua University Press and Springer-Verlag, Beijing, China.
3. Okiwa, M. and Tada, K. 1976, Appl. Phys. Lett. **29**, 491.
4. Huang, Z., Zhang, Q., and Whatmore, R. W. 1999, J. Appl. Phys. **86**, 1662.
5. Adachi, M., Matsuzaki, T. 1987, Jpn. J. Appl. Phys. **26**, 550.
6. Chu, H., Baik, H., Troccaz, M., Barbier, D. 1998, J. Mater. Sci. Lett., **17**, 255.
7. Haertling, G. H. 1999, J. Am. Ceram. Soc., **82**, 797.
8. Gerson, R. 1960, J. Appl. Phys. **31**, 188.
9. Takahashi, S. 1981, Jpn. J. Appl. Phys. **20**, 95.
10. Chang, J., Desu, S. B. 1996, J. Mater. Res. **9**, 955.
11. Boyle, T. J., Clem, P. G., Tuttle, B. A., Brennecka, G. L., Dawley, J. T., Rodriguez, M. A., Dunbar, T. D., Hammetter, W. F. 2002, J. Mater. Res. **17**, 871.
12. Araujo, C. A. P., Cuchlaro, J. D., McMillan, L. D., Scott, M. C., Scott, J. F. 1995, Nature, **374**, 627.
13. Lee, E. G., Lee, J. K., Lee, J. G., Kim, J. Y., and Jang, H. M. 1999, J. Mater. Sci. Lett., **18**, 1033.
14. Aurivillius, B. 1949, Arkiv. Kemi. **1**, 463.
15. Aurivillius, B. 1949, Arkiv. Kemi. **1**, 499.
16. Aurivillius, B. 1950, Arkiv. Kemi. **2**, 519.
17. Aurivillius, B. 1952, Arkiv. Kemi. **5**, 39.
18. Suzuki, M. 1996, J. Ceram. Soc. Jpn, Int. Ed., **103**, 1088.

19. Jones Jr., R. E., Maniar, P. D., Moazzami, R., Zurcher, P., Witowski, J. Z., Lii, Y. T., Chu, P., Gillespie, S. J., 1995, Thin Solid Films, **270**, 584.
20. Scott, J. F. and Araujo, C. A. P. 1989, Science, **246**, 1400.
21. Mihara, T., Yoshimori, H., Watanabe, H., and Araujo, C. 1995, Jap. J. App. Phys., **34**, 5233.
22. Ding, Y., Liu, J. S., Wang, Y. N. 2000, Appl. Phys. Lett., **76,** 103.
23. Ding, Y., Liu, J. S., Qin, H. X., Zhu, J. S. and Wang, Y. N. 2001, Appl. Phys. Lett., **78**, 4175.
24. Scott, J. F., 1997, Thin Film Ferroelectric Materials and Devices, edited by R. Ramesh, Kluwer, Norwell, MA, p.115.
25. Newnham, R. E., Wolfe, R. W., and Dorrian, J. F., 1971, Mater. Res. Bull., **6**, 1029.
26. Dorrian, J. F., Newnham, R. E., Smith, D. K., and Kay, M. I., 1971, Ferroelectrics, **3**, 17.
27. Watanabe, H., Mihara, T., Yoshimori, H., and Araujo, C. 1995, Jap. J. App. Phys., **34**, 5240.
28. Norden, B. 2000, Presentation speech for the Nobel Prize in Chemistry 2000.
29. Sze, S. M. 1985, Semiconductor devices, physics and technology, John Wiley & Sons, INC.
30. Limonov, M., Shantsev, D., Tajima, S., Yamanaka, A. 2002, Phys. Rev. B **65**, 024515.
31. Xu, Y. H. 1991, Ferroelectric Materials and Their Applications, Elsevier Science, Amsterdam.
32. Smollenskii, G. A., Isupanov, V. A., Agranovskya, A. I., 1961, Sov. Phys. Solid State, **3**, 651.
33. Newnham, R. E., Wolfe, R. W., Horsey, R. S., Diaz-Colon, F. A., and Kay, M. I., 1973, Mater. Res. Bull. **8**, 1183.
34. Lu, C. H. and Wen, C. Y., 1999, Mater. Res. Soc. Symp. **541**, 229.
35. Lu, C. H. and Wen, C. Y., 2000, J. Eur. Ceram. Soc. **20**, 739.
36. Takenaka, T., Gotoh, T., Mutoh, S., and Sasaki, T. 1995, Jap. J. App. Phys., **34**, 5384.
37. Forbess, M., Seraji, S., Wu, Y., Nguyen, C. P., and Cao, G. Z. 2000, Appl. Phys. Lett., **76**, 2934.
38. Wu, Y., Forbess, M., Seraji, S., Limmer, S., Chou, T., Nguyen, C., and Cao, G. 2001, J. Appl. Phys., **90**, 5296.
39. Suzuki, M. 1995, J. Ceram. Soc. Jpn. **103**, 1088.
40. Isupov, V. A. 1997, Inorg. Mater. (Transl. Neorg. Mater.) **33**, 936.
41. Moulson, A. J., and Herbert, J. M., 1990, Electroceramics, Chapman and Hall, London.
42. Chen, A., Zhi, Y., and Cross, L. E. 2000, Phys. Rev. B. **62**, 228.
43. Zhi, Y., Chen, A., Vilarinho, P. M., Mantas, P., and Baptista, J. L., 1998, J. Appl. Phys., **83**, 4874.
44. Waser, R. 1991, J. Am. Ceram. Soc., **74**, 1934.
45. Weast, R. C. and Astle, M. J. 1974, edited CRC Handbook of Chemistry and Physics, 61st edi. (CRC, Boca Raton, FL).
46. Park, B. H., Kang, B. S., Bu, S. D., Noh, T. W., Lee, J., and Jo, W. 1999, Nature, **401**, 682.
47. Melgarejo, R. E., Tomar, M. S., Bhaskar, S., Dobal, P. S., and Katiyar, R. S. 2002, Appl. Phys. Lett. **81**, 2611.
48. Kojima, T., Sakai, T., Watanabe, T., Funakubo, H., Saito, K., and Osada, N. 2002, Appl. Phys. Lett. **80**, 2746.
49. Chon, U., Kim, K., Jang, M., and Yi, G. C. 2001, Appl. Phys. Lett., **79**, 3137.
50. Pauling, L. 1960, The Nature of the Chemical Bond, 3rd ed., Cornell University Press.
51. Okuwada, K., Nakamura, S., Nozawa, H. 1999, J. Mater. Res., **14**, 855.
52. Wu, Y., Nguyen, C., Seraji, S., Forbess, M. J., Limmer, S. J., Chou, T. P., and Cao, G. Z. 2001, J. Am. Ceram. Soc., **84**, 2882.
53. Wu, Y., and Cao, G. Z. 2000, J. Mater. Res., **15**, 1583.
54. Wu, Y., and Cao, G. Z. 1999, Appl. Phys. Lett., **75**, 2650.
55. Wu, Y., and Cao, G. Z. 2000, J. Mater. Sci. Lett., **19**, 267.
56. Wu, Y., Forbess, M. J., Seraji, S., Limmer, S. J., Chou, T. P., and Cao, G. Z. 2001, J. Appl. Phys., **89**, 5647.
57. Wu, Y., Forbess, M. J., Seraji, S., Limmer, S. J., Chou, T. P., and Cao, G. Z. 2001, Mater. Sci. Eng. B **86**, 70.

58. Kuo, C., Chen, C., and Lin, I. 1998, J. Am. Ceram. Soc., **81**, 2942.
59. Varma, K. B. R., and Prasad, K. V. R., 1996, J. Mater. Res., **11**, 2288.
60. Chen, S., Lan, B., and Taso, C. 2002, J. Appl. Phys., **91**, 10032.
61. Irie, H., Miyayama, M., and Kudo, T. 2001, Jap. J. App. Phys., **40**, 239.
62. Atsuki, T., Soyama, N., Yonezawa, T. and Ogi, K. 1995, Jap. J. App. Phys., **34**, 5096.
63. Miura, K. and Tanaka, M. 1998, Jap. J. App. Phys., **37**, 2554.
64. Torii, Y., Tato, K., Tsuzuki, A., Hwang, H. J., Dey, S. K. 1998, J. Mater. Sci. Lett., **17**, 827.
65. Ding, Y., Liu, J. S., Zhu, J. S. and Wang, Y. N. 2002, J. Appl. Phys., **91**, 2255.
66. Noguchi, T., Hase, T., and Miyasaka, Y. 1996, Jpn. J. Appl. Phys. **35**, 4900.
67. Koiwa, I., Kanehara, T., Mita, J., Iwabuchi, T., Osaka, T., Ono, S., and Maeda, M. 1996, Jpn. J. Appl. Phys. **35**, 4946.
68. Koiwa, I., Okada, Y., Mita, J., Hashimoto, A., and Sawada, Y. 1997, Jap. J. App. Phys., **36**, 5904.
69. Noda, M., Matsumuro, Y., Sugiyama, H., and Okuyama, M. 1999, Jap. J. App. Phys., **38**, 2275.
70. Wu, Y., Limmer, S. J., Chou, T. P., Nguyen, C., and Cao, G. Z. 2002, J. Mater. Sci. Lett., **21**, 947.
71. Duran-Martin, P., Castro, A., Millan, P., and Jimenez, B. 1998, J. Mater. Res., **13**, 2565.
72. Noguchi, Y., Miwa, I., Goshima, Y., and Miyayama, M. 2000, Jap. J. App. Phys., **39**, L259.
73. Wan, D. W., Wang, J., Ng, S. C., Gan, L. M. 1999, J. Mater. Res., **14**, 537.
74. Sai Sunder, V. V. S. S., Halliyal, A., and Umarji, A. M. 1995, J. Mater. Res. **10**, 1301.
75. Kumar, M.M., Srinivas, A., Kumar, G.S., Suryanarayana, S.V. 1999, J. Phys.: Condensed Mater. **11**, 8131.
76. Ko, T. 1997, Comparative structural study on the system $Bi_4Ti_3O_{12}$·ABO_3 (ABO_3 = $CaTiO_3$, $BiFeO_3$ and $BaTiO_3$), ISIS experimental report (RB 7742).
77. Gu, H., Xue, J., and Wang, J. 2001, Appl. Phys. Lett., **79**, 2061.
78. Kijima, T., and Matsunaga, H., 1998, Jap. J. Appl. Phys., **37**, 5171.
79. Kijima, T., Ishiwara, H. 2002, Jap. J. App. Phys., **41**, L716.
80. Irifune, T., and Ringwood, A. E., 1993, Earth Planet Sci. Lett., **117**, 101.
81. Toyoda, M., Hamaji, Y., Tomono, K., and Payne, D. 1994, Jpn. J. Appl. Phys. **33**, 5543.
82. Millan, P., Ramirez, A., Castro, A. 1995, J. Mater. Sci. Lett. **14**, 1657.
83. Millan, P., Castro, A., and Torrance, J. 1993, Mater. Res. Bull. **28**, 117.
84. Tabata, H., Tanaka, H., and Kiwai, T., 1995, Jap. J. Appl. Phys., **34**, 5146.
85. Watanabe, K., Tanaka, M., Sumitomo, E., Katori, K., Yagi, H. and Scott, J. F. 1998, Appl. Phys. Lett. **73**, 126.
86. Desu, S. B., and Vijay, D. P., 1995, Mater. Sci. & Engr. B **32**, 83.
87. Wu, Y., Ohuchi, F. S., Cao, G. Z. 1999, Mater. Res. Soc. Symp. Proc. **541** (Ferroelectric Thin Films VII), 253.
88. H. N. Lee, S. Senz, N. D. Zakharov, C. Harnagea, A. Pignolet, D. Hesse, and U. Gösele, Appl. Phys. Lett. **77**, 3260 (2000).
89. Osaka, T., Yoshie, T., Hoshika, T., Koiwa I., Sawada, Y., and Hashimoto, A. 2000, Jap. J. App. Phys., **39**, 5476.
90. Koiwa, I., Kanehara, T., Mita, J., Iwabuchi, T., Osaka, T., and Ono, S. 1997, Jap. J. App. Phys., **36**, 1597.
91. Nakamura, T., Muhammet, R., Shimizu, M. and Shiosaki, T. 1993, Jpn. J. Appl. Phys., **32**, 4086.
92. Tani, K., Yamanobe, T., Matsuhashi, H., and Nishikawa S. 1997, Jap. J. App. Phys., **36**, 1460.
93. Sun, Y., Chen, Y., Gan, J. and Hwang, J. 2002, Appl. Phys. Lett., **81**, 3221.
94. Yamaguchi, M., and Nagatomo, T. 1998, Jap. J. App. Phys., **37**, 5166.
95. Wu, W., Fumoto, K., Oishi, Y., Okuyama, M., and Hamakawa Y. 1995, Jap. J. App. Phys., **34**, 5141.